Elastic properties of floating sea ice from air-coupled flexural waves

Rowan Romeyn[1,2], Alfred Hanssen[1,2], Bent Ole Ruud[2,3], Tor Arne Johansen[2,3,4]

[1]Department of Geosciences, University of Tromsø – The Arctic University of Norway, 9037 Tromsø, Norway
[2]Research Centre for Arctic Petroleum Exploration (ARCEx)
5 [3]Department of Earth Science, University of Bergen, 5007 Bergen, Norway
[4]The University Centre in Svalbard (UNIS), 9171 Longyearbyen, Norway

Correspondence to: Rowan Romeyn (rowan.romeyn@uit.no)

Abstract. Air-coupled flexural waves appear as wave trains of constant frequency that arrive in advance of the direct air-wave
10 from an impulsive source travelling over a floating ice sheet. The frequency of these waves varies with the flexural stiffness
of the ice sheet, which is controlled by a combination of thickness and elastic properties. We develop a theoretical framework
to understand these waves, utilizing modern numerical and Fourier methods to give a simpler and more accessible description
than the pioneering, yet unwieldly analytical efforts of the 1950's. Our favoured dynamical model can be understood in terms
of linear filter theory and is closely related to models used to describe the flexural waves produced by moving vehicles on
15 floating plates. We find that air-coupled flexural waves are a robust feature of floating ice-sheets excited by impulsive sources
over a large range of thicknesses, and we present a simple closed-form estimator for the ice thickness. Our study is focussed
on first-year sea ice of ~20-80 cm thickness in Van Mijenfjorden, Svalbard, that was investigated through active source seismic
experiments over four field campaigns in 2013, 2016, 2017 and 2018. The air-coupled flexural frequencies for sea-ice in this
thickness range are ~60-240 Hz. While air-coupled flexural waves for thick sea-ice have received little attention, the higher
20 frequencies associated with thin ice on fresh water lakes and rivers are well known to the ice-skating community and have
been reported in popular media. Estimation of ice physical properties, following the approach we present, may allow improved
surface wave modelling and wavefield subtraction in reflection seismic studies where flexural wave noise is undesirable. On
the other hand, air-coupled flexural waves may also permit non-destructive continuous monitoring of ice thickness and flexural
stiffness using simple, relatively inexpensive microphones located in the vicinity of the desired measurement location, either
25 above the ice-sheet or along the shoreline. In this case, naturally forming cracks in the ice may be an appropriate impulsive
source capable of exciting flexural waves in floating ice sheets in a passive monitoring context.

1 Introduction

The term "air-coupled flexural wave" was coined by Press et al. (1951) to describe wave trains of constant frequency, varying
with the flexural stiffness of a floating ice sheet, that arrive in advance of the pressure waves produced by an explosive source.
30 The coupling in the case of "air-coupled flexural waves" is set up between pressure waves in air and flexural waves in the solid
that have phase velocity equal to the speed of sound in air. Flexural waves propagating in a floating ice sheet are a class of

surface waves analogous to Rayleigh waves on the surface of elastic solids, or bending waves in rods and beams. Greenhill (1886) published one of the earliest mathematical descriptions of flexural waves in a floating ice sheet and also discussed the concept of coupling between waves in air and water, which was further developed in Greenhill (1916). Several studies have

35 used the dispersion of ice flexural waves to estimate ice elastic parameters, of these we highlight in particular the early work of Ewing and Crary (1934) and the study of Yang and Yates (1995) that highlights the usefulness of transform methods in this field. The air-coupled flexural waves arrive in advance of the air wave because the group velocity of the flexural waves is larger than the phase velocity (Press et al., 1951).

40 Despite their commendable efforts to develop a theoretical foundation for the air-coupled flexural wave (Press and Ewing, 1951b), the term has not been widely used since the initial investigation period in the 1950's and the study of Hunkins (1960). This may be because the theory developed by Press and Ewing (1951b) is cumbersome, being built-up using demanding analytical integration methods at a time when computing power to handle more convenient numerical methods did not exist. We think this is unfortunate since the term "air-coupled flexural wave" gives a concise description of the physical mechanism

45 that produces these waves. Furthermore, their constant frequency is attractive from an experimental standpoint, being easier to estimate from real data than the precise time-frequency evolution of the highly dispersive flexural wave train. Air-coupled flexural waves may therefore provide a simple and effective means to estimate the flexural rigidity of a floating ice sheet and to study variation in ice thickness, for the case where the elastic properties of the ice sheet are assumed or independently estimated.

50 **1.1 A convergence of fields**

Coupling between air and surface waves is not limited to the case of a floating ice sheet and can be anticipated in all cases where the surface wave phase velocity is equal to the speed of sound in air (Haskell, 1951; Press and Oliver, 1955). For example, one of the strongest air waves ever recorded was produced by the volcanic eruption of Krakatoa in 1883, which travelled around the globe three times. It was not until the concept of air-coupled surface waves emerged that the extent of

55 tidal waves associated with the eruption could be adequately explained, where previous explanations had to invoke multiple coincidental local earthquakes at different locations to explain the observed arrivals of gravity waves in the ocean (Ewing and Press, 1955). The correlation of the major tide-gauge disturbances with the arrival of the first or second airwave from the Krakatoa eruption has since been explained by waves propagating in a realistically coupled atmosphere-ocean system (Garrett, 1970; Harkrider and Press, 1967). Within the paradigm of air-wave coupling, it is straightforward to understand why tide-

60 gauge disturbances in the English Channel correlated with the arrival of the second air wave from Krakatoa, which arrived from the seaward side, rather than the first air wave that arrived from the landward side (Ewing and Press, 1955).

The idea of coupling between air and surface waves also exists in other fields, under different terminological guises. In the field of structural acoustics, the frequency at which the free bending wave becomes equal to the speed of sound in air is called

65   the critical frequency and is closely related to the coincidence frequency, where the speeds of the free and forced bending

waves are equal (Renji et al., 1997). An understanding of the coupling between air waves and bending waves in structures

therefore permits the design of advanced components like the honeycomb sandwich composite panels that are used in aerospace

applications, where one may wish to minimise the vibration response of the panels to acoustic excitation (Renji et al., 1997).

Air coupled waves are also utilised in non-contact applications of non-destructive testing of engineered structures, like concrete

70   slabs, allowing improved testing efficiency compared to applications using sensors bonded to the surface (e.g. Zhu, 2008).

At the coincidence frequency, a plate excited to vibration by travelling acoustic waves is acoustically transparent and

maximally transmitting (Bhattacharya et al., 1971). A fascinating manifestation of this property is well known in the world of

wild ice-skating. Chasing perfectly smooth, newly frozen ice, typically in the ~4 cm thickness range, these skaters flex the ice

75   with their bodyweight and crack it with their skates. The acoustic waves produced by this cracking propagate over the ice

surface and are maximally transmitted due to constructive interference with ice flexural waves at the frequency where the

phase velocity of the flexural waves in the ice is equal to the speed of sound in air. When the ice is thin, this occurs in the

audible frequency range and produces striking sounds reminiscent of whale song or science fiction films, that have captured

significant media attention (Griffin, 2018; Rankin, 2018). This phenomenon is clearly a direct analogue of the air-coupled

80   flexural waves of Press et al. (1951), occurring simply within a different part of the frequency/flexural stiffness spectrum.

1.2 A general theory - moving loads on floating plates

We now consider the closely related topic of moving vehicles travelling over floating ice sheets. The topic of moving loads on

floating plates has received considerable attention due to the importance of roads on floating sea, river and lake ice that are

traversed by vehicles from snow scooters to semi-trailers (Takizawa, 1988; Van der Sanden and Short, 2017; Wilson, 1955).

85   Aircraft take-off and landing on floating ice (Matiushina et al., 2016; Yeung and Kim, 2000) or large man-made floating

structures (Kashiwagi, 2004) has also received significant attention. A major focus of many of these studies is the so-called

critical load speed, where the load speed coincides simultaneously with the flexural phase and group velocities and the ice

deflection can grow very large over time (Wilson, 1955). In general, these studies are geared towards understanding the critical

load speed so that vehicular transit at that speed may be avoided (e.g. Schulkes and Sneyd, 1988). Further studies have shown

90   that the build-up of large enough deflections to break the ice may be limited by 2D spreading (Nugroho et al., 1999), viscous

effects (Wang et al., 2004), acceleration/deceleration through the critical speed (Miles and Sneyd, 2003) and/or nonlinearities

(Dinvay et al., 2019). Interestingly, a complementary field of study also exists that focuses on leveraging the resonant flexural

waves produced by moving hovercraft to enhance their effectiveness as icebreakers (Hinchey and Colbourne, 1995; Kozin et

al., 2017). Submarines surfacing in ice covered waters may also seek to weaken or break the ice before surfacing by creating

95   flexural gravity waves (Kozin and Pogorelova, 2008), which has been studied via an adaption of the theoretical framework to

include moving loads in the water column under a floating plate.

We propose that the air-coupled flexural wave phenomenon is simply a special case of the more general paradigm of moving loads on floating plates, where the load speed is equal to the speed of sound in air. Furthermore, we hope to highlight the close physical relationship between phenomena spanning from Arctic seismic experiments to wild ice-skating, ice-roads, floating runways, structural acoustics and the eruption of Krakatoa. Our study was also motivated from the pragmatic standpoint that the constant air-coupled flexural wave frequency is relatively straightforward to measure and can be related directly to ice thickness and rigidity. While other studies have focussed on measuring the dispersion of ice flexural-waves in order to estimate ice physical properties (DiMarco et al., 1993; Yang and Yates, 1995), we present an alternative that is straightforward to implement and effective for both point and line seismic sources.

2 Study area and data acquisition

In this study we investigate a series of active-source seismic experiments conducted in the innermost part of Van Mijenfjorden, on the island of Spitsbergen, in the high-Arctic Svalbard archipelago. The experiments were conducted during the spring season, when sea-ice is best developed, in 2013, 2016, 2017 and 2018, as illustrated in Figure 1. Detonating cord of the type "Nobelcord", containing 40g Pentrit (PETN) per meter, was laid on the ice surface in various lengths or coiled into point like charges, to provide the seismic source. An example of the detonation of a point charge is shown in Figure 2. As indicated by the photo, these seismic sources produce a strong air-wave that propagates radially over the ice surface, in addition to energy that travels horizontally through the ice, or downwards through the water column where it may be reflected back to the surface by layers of contrasting acoustic impedance. The sum of all of these modes of propagation gives the complex seismic wavefield that was recorded using line arrays of geophones installed on the ice surface. For the majority of the experiments, the geophones were arranged in-line with the source, but we also include oblique arrangements from the 2013 campaign that employed a cross type array (see Figure 1).

The main purpose of these experiments was to test different acquisition designs for reflection seismic surveying of sub-seabed sediments, as reported by Johansen et al. (2019), an objective which is made difficult by the flexural wave energy propagating through the ice. Various source and receiver arrangements were tested including airguns, hydrophones and ocean bottom seismometers. However, in this study we focus on the subset of experiments employing explosive sources and vertical-component gimballed geophones deployed on top of the ice. This acquisition setup is operationally the simplest under field conditions, but leads to the strongest recordings of ice flexural waves. While the flexural wave energy is regarded as bothersome coherent noise from the context of sub-seabed reflection surveying, it constitutes the primary signal in the present study and allows us to estimate the flexural stiffness of the floating ice.
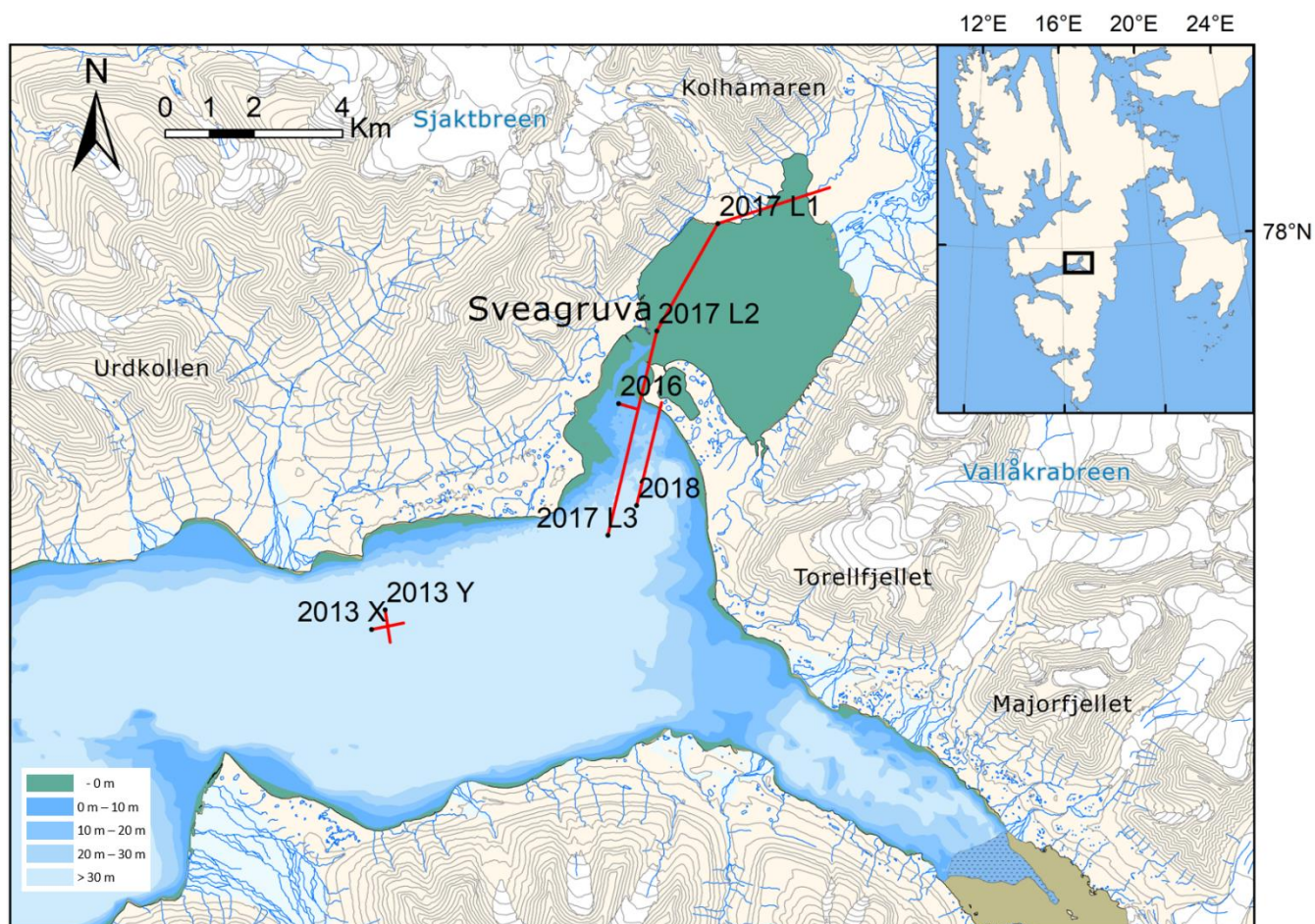
Figure 1 – 1:100 000 scale map of the study area in the innermost part of Van Mijenfjorden, Spitsbergen indicating the seismic
130 **profiles collected during field campaigns in 2013, 2016, 2017 & 2018. The inset map indicates the position relative to the Svalbard**
archipelago. The contour interval on land is 50 m. Map data © Norwegian Polar Institute (http://npolar.no, last access: 25/06/2020).

Figure 2 – Photo taken during the 2013 field campaign showing the explosive seismic source. The line of seismic receivers is marked
with red poles (Photo: Robert Pfau).

3 Theory

3.1 General wavefield solution

In this work we consider a thin elastic plate resting on an incompressible inviscid fluid of finite depth, that corresponds to the widely used "simplest acceptable" mathematical model advocated by Squire et al. (1996). The plate extends infinitely along the horizontal x and y axes and the vertical axis, z, is positive downwards with its origin at the upper undisturbed water surface. We impose the constraint that the fluid must satisfy the Laplace equation, $\nabla^2\phi = 0$, where ϕ is the velocity potential in the fluid. In addition, we impose a non-cavitation condition at the surface, $\frac{\partial\phi}{\partial z}\big|_{z=0} = \frac{\partial\zeta}{\partial t}$, and a normal flow condition at the sea bottom, $\frac{\partial\phi}{\partial z}\big|_{z=H} = 0$, where $\zeta(x,y,t)$ is the vertical deflection of the plate's neutral surface and H is the water depth. The linear spatiotemporal dynamics of the system is described by the partial differential equation (e.g., Squire et al., 1996)

$$D\nabla^4\zeta + \rho_l h \frac{\partial^2\zeta}{\partial t^2} + \rho_w g\zeta = -\rho_w \frac{\partial\phi}{\partial t}\Big|_{z=0} - f(x,y,t). \tag{1}$$

Here, $D = \frac{Eh^3}{12(1-\sigma^2)}$ is the plate flexural stiffness, E is Young's modulus, h is the plate thickness, σ is Poisson's ratio, ρ_w is the water density, ρ_l is the plate density, $g = 9.81$ m.s^{-2} is the acceleration due to gravity and $f(x,y,t)$ is the applied external spatiotemporal force.

In order to solve for the spatiotemporal deflection of the ice surface, we apply the 3D Fourier transform (FT) defined as

$$P(k_x, k_y, \omega) = \iiint p(x,y,t)e^{i(k_x x + k_y y - \omega t)}dx\, dy\, dt, \tag{2}$$

for an arbitrary spatiotemporal function $p(x,y,t)$. The wave number vector $\boldsymbol{k} = \begin{bmatrix} k_x \\ k_y \end{bmatrix}$ is decomposed in the x and y directions, $k^2 = |\boldsymbol{k}|^2 = k_x^2 + k_y^2$, and i denotes the imaginary unit. By applying the FT defined in Eq. (2) to the spatiotemporal fields in Eq. (1), we find that the solution for the deflection in Fourier space is given by

$$Z(k_x, k_y, \omega) = -\frac{F(k_x, k_y, \omega)}{G(k_x, k_y, \omega)}, \tag{3}$$

where $G(k_x, k_y, \omega) = Dk^4 + \rho_w g - \rho_l h\omega^2 - \left(\frac{\rho_w \omega^2}{k}\right)\coth(kH)$. Recalling linear filter theory, the form of Eq. (3) highlights that the floating ice plate simply acts as a linear filter on an arbitrary spatiotemporal input signal. This formulation is also attractive because the physical significance of the different terms in the denominator are clearly preserved: Dk^4 expresses the bending forces in the plate, $\rho_w g$ is due to the plate buoyancy, $\rho_l h\omega^2$ is the plate acceleration and $\left(\frac{\rho_w \omega^2}{k}\right)\coth(kH)$ arises due to the constraint of finite water depth.

The general solution for of the resulting spatiotemporal deflection wavefield, $\zeta(x,y,t)$, is then given by the full three-dimensional inverse FT of $Z(k_x, k_y, \omega)$ as

$$\zeta(x,y,t) = -\frac{1}{(2\pi)^3} \iiint \frac{F(k_x,k_y,\omega)}{G(k_x,k_y,\omega)} e^{-i(k_x x + k_y y - \omega t)} dk_x \, dk_y \, d\omega. \tag{4}$$

3.2 Ring delta function source for radial symmetry

165   To exploit spatial symmetry and reduce the dimensionality of the problem, we approximate the explosive source as a ring-shaped Dirac delta pulse expanding outwards from the origin with radial symmetry. This allows us to reduce the spatial dimensionality of the problem by using the radial coordinate $r = \sqrt{x^2 + y^2}$ and representing the propagating air wave source using the ring delta function,

$$f(r,t) = -\frac{1}{2\pi r} \delta(r - c_{air} t), \tag{5}$$

170   where c_{air} is the speed of sound in air. By performing a partial Fourier transform of Eq. (5) with respect to time t, we obtain the spatio-frequency representation of the source as

$$F(r,\omega) = \int_{-\infty}^{\infty} f(r,t) e^{-i\omega t} dt = -\frac{1}{2\pi r c_{air}} e^{-i\omega r / c_{air}}, \tag{6}$$

so the spatio-frequency deflection wavefield can be written as

175    $$Z(r,\omega) = -\frac{F(r,\omega)}{G_0(\omega)}, \tag{7}$$

where

$$G_0(\omega) = D(\frac{\omega}{c_{air}})^4 + \rho_w g - \rho_l h \omega^2 - (c_{air} \rho_w \omega) \coth\left(\frac{\omega H}{c_{air}}\right). \tag{8}$$

The spatiotemporal deflection wavefield in radial coordinates then becomes

$$\zeta(r,t) = -\frac{1}{2\pi} \int_{-\infty}^{\infty} \frac{F(r,\omega)}{G_0(\omega)} e^{i\omega t} d\omega. \tag{9}$$

180   When evaluating Eq. (9) numerically, we substitute $G_0(\omega) \to G_0(\omega + i\gamma)$, where $\gamma > 0$, which avoids dividing by zero and gives a tuneable heuristic damping parameter for wave attenuation and dissipation.

3.3 Dispersion relation

The dispersion relation for the propagating wavefield in the ice sheet is given by the wavenumber and frequency pairs that satisfy the equation

185    $$G(k,\omega) = 0. \tag{10}$$

The solution of Eq. (10) gives the general dispersion relation (e.g., Squire et al., 1996)

$$\omega^2 = \frac{D k^5 / \rho_w + g k}{k h \frac{\rho_l}{\rho_w} + \coth(kH)}. \tag{11}$$

This solution of the dispersion relation is complete in the sense that it retains all physical mechanisms included in the dynamical model Eq. (1). However, at typical vehicle speeds that have been the main focus of moving load on floating plate studies, the

190   flexural waves produced by the moving load have wavelengths much larger than the thickness of the floating plate. It has thus

been common for these studies to neglect the effect of the plate acceleration (e.g. Schulkes and Sneyd, 1988; Wang et al., 2004). Under this assumption the dispersion relation, Eq. (11), can be approximated by

$$\omega^2 \approx \left(\frac{Dk^4}{\rho_w g} + 1\right) gk \tanh(kH). \tag{12}$$

Another common assumption is to assume infinite water depth, H, which causes the hyperbolic tangent term to approach unity.

195   However, when we consider loads moving at the speed of sound in air, plate flexural waves with much shorter wavelengths are resonant and it becomes important to retain the plate acceleration term in order to accurately estimate the frequency of air-coupled flexural wave. The common approximations that are valid at typical vehicle speeds may lead to significant inaccuracies when estimating physical properties of the floating ice sheet from estimates of air-coupled flexural wave frequency.

200
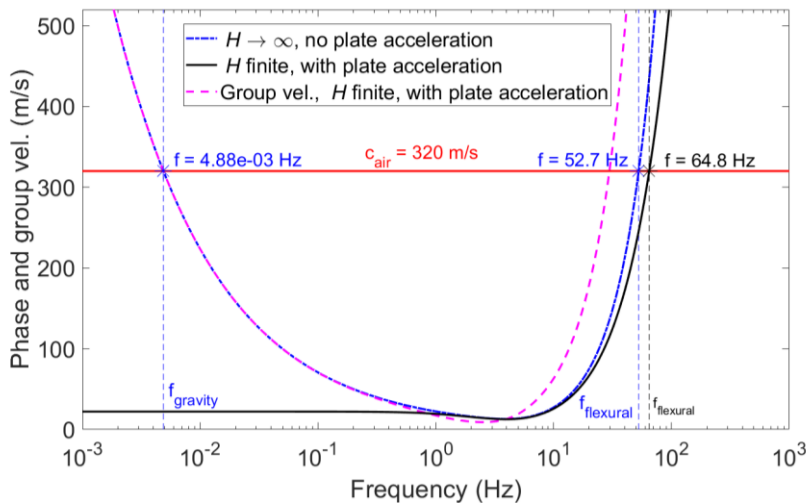
Figure 3 – Comparison of simplified dispersion relation neglecting water depth and plate acceleration (blue, Eq. 12) with the full dispersion relation including these effects (black, Eq. 11) for realistic sea-ice physical properties h = 0.74 m, E = 2.5 GPa, σ = 0.33, ρ_w = 1027 kg/m³, ρ_l = 931 kg/m³ and H = 50 m.

205   Figure 3 compares the full dispersion relation (Eq. (11)) with the approximation that neglects water depth and plate acceleration (Eq. (12)). Air-coupled waves are excited where the phase velocity is equal to the speed of sound in air, shown as the horizontal red line in Fig. 3. With finite water depth H (black line in Fig. 3), we see that only flexural waves are coupled to the air wave. While gravity waves may couple to the air-wave for the case of an infinite fluid (blue dashed line in Fig. 3), their extremely low frequency of ~0.005 Hz would likely be difficult to measure in practice. The air-coupled flexural waves arrive in advance

210   of the air wave because the group velocity, $\partial\omega/\partial k$, is larger than the phase velocity for a given frequency (magenta dashed line in Fig. 3). The air-coupled flexural frequency is insensitive to water depths >2 m, in this example, but is significantly affected by the plate acceleration term. Including the effect of plate acceleration increases the air-coupled flexural frequency by ~12 Hz (~23%) using physical properties relevant to our field data. While studies of moving vehicles on floating plates

may safely ignore the effect of plate acceleration, we show that is important to include it when the load is moving at the speed

215   of sound in air.

4 Methodology

Using air-coupled flexural waves to study the properties of floating ice is relatively straightforward because one simply needs to extract the segment of the timeseries that directly precedes the air-wave arrival and estimate the constant frequency of the air-coupled flexural waves, that are typically the dominating wavemode in terms of amplitude for this segment. The air-coupled

220   flexural frequency can then be directly related to the physical properties of the floating ice sheet using the dispersion relation introduced in the previous section.

4.1 Air wave arrival and velocity estimation

Since the arrival time of the air wave increases linearly with horizontal offset between the seismic source and receiver, we can estimate its arrival time and velocity using the linear Radon transform, that is also referred to as the slant-stack or $\tau - p$

225   transform (Yilmaz, 2001). For a given shot gather (see Figure 4a), we compute the linear Radon transform and estimate the velocity (c_{air}) and intercept (t_{int}) corresponding to the air wave by picking the local maximum of the transform magnitude (see Figure 4b). The estimated arrival time of the air wave, t_{air}, is then given by, $t_{air} = \frac{d}{c_{air}} + t_{int}$, where d is the source to receiver offset.

4.2 Thomson multitaper estimation of air-coupled flexural frequency

230   The frequency of the air-coupled flexural wave is estimated from segments of the recorded timeseries which precede the arrival of the air-wave (see Figure 4c). We take the derivative of the trace to suppress low frequencies and linearly increase the gain of high frequencies and apply a Hamming window taper. For each trace the Thomson multitaper power spectral density (Thomson, 1982) is then estimated using a time-half bandwidth product of two and a zero-padded Fourier transform length of 4096. The air-coupled flexural frequency (see Figure 4d) is then estimated from the multitaper power spectral density

235   maximum. We only attempt to estimate the air-coupled flexural frequency for source to receiver offsets greater than 125 m because higher-velocity sub-seabed reflections arrive around the same time as the air wave and create too much interference at nearer offsets (see Figure 5).
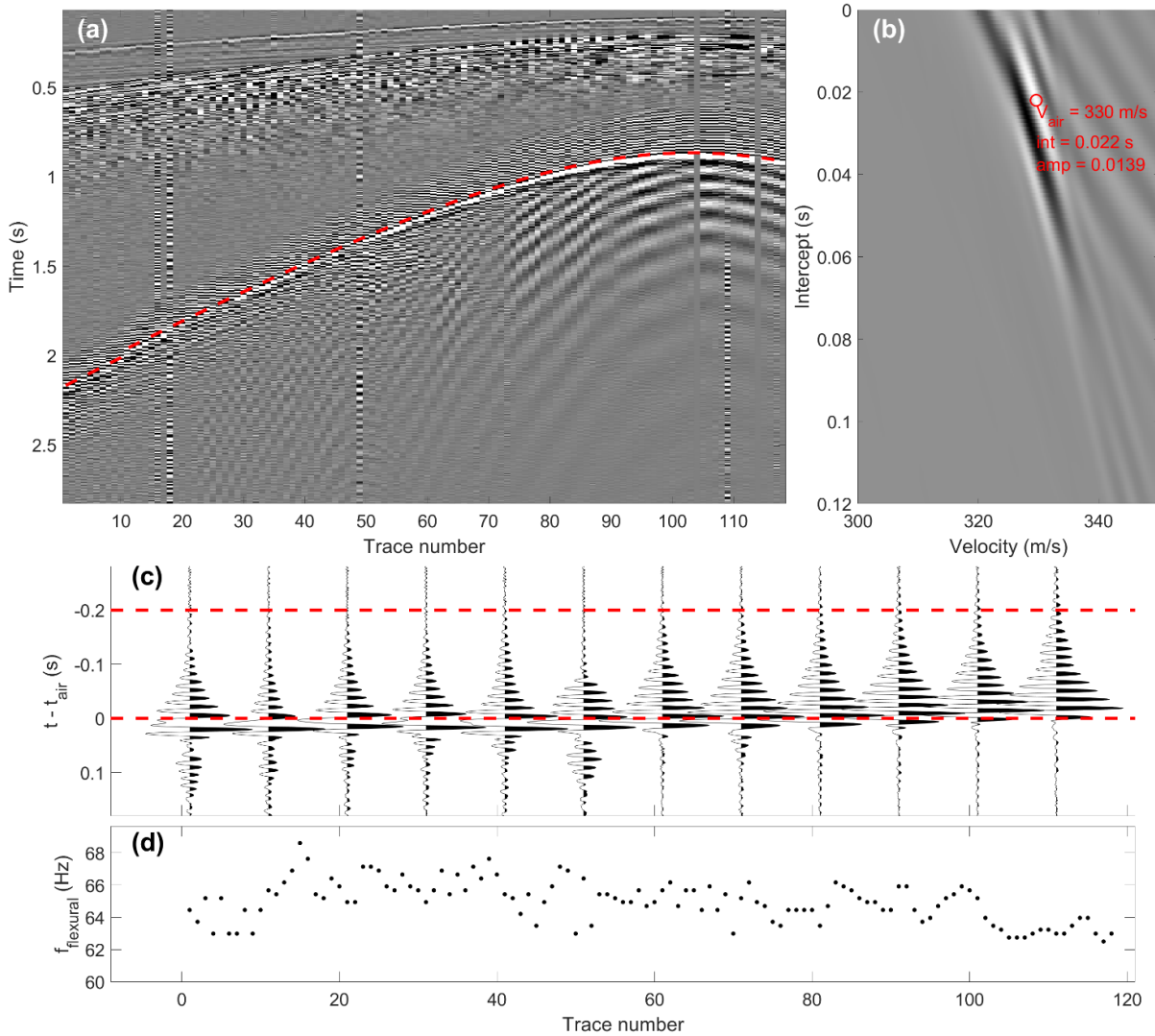
Figure 4 – Example of air-coupled flexural wave frequency estimation. (a) shot gather with air wave arrival indicated, (b) air wave arrival time and velocity is estimated by picking the local maximum of the linear radon transform, (c) waveform plot for every 10th trace indicating the frequency estimation window, (d) air-coupled flexural frequency estimated by the multitaper method.

4.3 Closed-form estimator of ice thickness

Once we have estimated the frequency of the air-coupled flexural wave (ω_f) we can estimate the ice thickness using the dispersion relation (Eq. (11)) rearranged as,

$$\frac{Eh^3 k_f{}^5}{12\rho_w(1-\sigma^2)} + gk_f = \omega_f{}^2 \left[k_f h \frac{\rho_l}{\rho_w} + \coth\left(k_f H\right)\right], \tag{13}$$

where $k_f = \omega_f / c_{air}$ is the wavenumber corresponding to the air-coupled flexural wave. The inclusion of the plate acceleration term means that we are left with a non-linear relation for the plate thickness h in terms of the plate elastic properties and the

constant flexural frequency and wavenumber. We may either estimate the ice thickness by nonlinear numerical optimisation
250 of Eq. (13), using e.g. the bisection method, or we may rearrange Eq. (13) to give the cubic polynomial form,

$$\left(\frac{Ek_f^5}{12\rho_w(1-\sigma^2)}\right)h^3 - \left(\omega_f^2 k_f \frac{\rho_l}{\rho_w}\right)h + gk_f - \omega_f^2 \coth(k_f H) = 0 ,$$ (14)

which has one real, positive root corresponding to the plate thickness h. It is possible to derive a compact closed-form analytical
255 solution for the cubic polynomial, following the approach of Nickalls (1993), leading to the following estimator,

$$h = 2\sqrt{\frac{b}{3a}}\cos\left[\frac{1}{3}\cos^{-1}\left(\frac{-3\sqrt{3}}{2}a^{1/2}b^{-3/2}c\right)\right] ,$$ (15)

where $a = \frac{Ek_f^5}{12\rho_w(1-\sigma^2)}, b = \omega_f^2 k_f \frac{\rho_l}{\rho_w}$ and $c = gk_f - \omega_f^2 \coth(k_f H)$. For the purpose of quality control, we have confirmed

that nonlinear numerical optimisation of Eq. (13), polynomial root finding of Eq. (14) and the closed form Eq. (15) all give
260 identical results.

5 Results

Air-coupled flexural waves appear to be a robust part of the wavefield excited by impulsive loads on floating sea-ice and were
observed for all four field campaigns. Furthermore, Figure 5 illustrates that since the air-coupled flexural waves precede the
arrival of the air wave they are recorded equally well for both point and line sources. This is significant because much of our
265 field data employed line sources in order to attenuate the trailing low-frequency flexural waves that are an unwanted noise
component from the perspective of reflection seismic surveying (Johansen et al., 2019).

**Table 1 – Summary of ice thicknesses (h) estimated from air-coupled flexural waves compared to the range of ice thicknesses
measured in boreholes drilled through the ice. MAD = median absolute deviation.**

Field season	h median air-coupled flexural wave estimate (cm)	MAD (cm)	h measured in boreholes (cm)	Young's modulus E (GPa)	Poisson's ratio σ	ρ_{ice} (kg.m^{-3})	ρ_{water} (kg.m^{-3})	Water depth H (m)
2013	76.3	2.6	74-79					
2016	34.3	2.6	30-40	2.5	0.33	931	1027	50
2017	56.8	4.0	30-75					
2018	30.3	2.4	20-40					

270
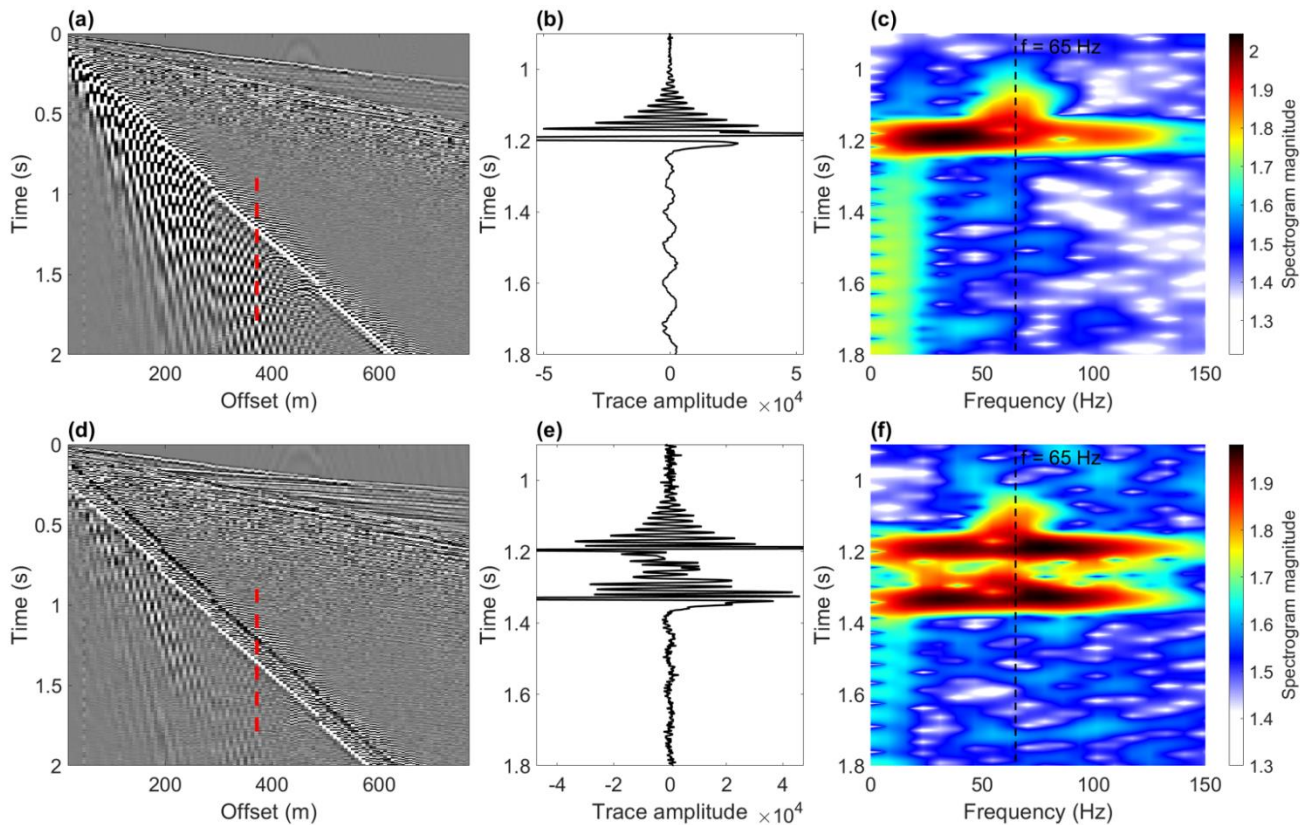
Figure 5 – Example shot gathers for (a) a point charge and (d) a 50m long, detonating cord line source, (b) and (e) show illustrative time series enlarged around the air wave arrival, (c) and (f) show spectrograms for the time series (b) and (e). The air-coupled flexural wave arrives in advance of the broadband air-wave with constant frequency of ~65 Hz.

275

As summarised in Table 1, ice thicknesses calculated using Eq. (15) from the estimated air-coupled flexural frequencies and air-wave velocities show very good agreement with ice thicknesses measured in boreholes. Notably, this good agreement was achieved across all four field seasons with a single set of elastic properties, that are realistic for sea ice. This indicates that the first-year sea ice which forms in Van Mijenfjorden has relatively constant macro-scale elastic properties for the range of

280   observed thicknesses from 20-80 cm, despite significant differences in surface weather and ice conditions during the experiments. The value of Young's modulus that we assume, E=2.5 GPa, is within the range of 1.7-5.7 GPa reported by Timco and Weeks (2010) for dynamic Young's modulus in first-year sea ice. The range of Young's modulus reported by Timco and Weeks (2010) would produce a variation of ~60% in air-coupled flexural frequency and is the most important parameter after ice thickness. The value of dynamic Poisson's ratio has been reported to fall in the range 0.33-0.39 (Timco and Weeks, 2010),

285   which would produce a variation of ~2% in air-coupled flexural frequency and is therefore of secondary importance. If we had opted to use a Poisson's ratio of 0.39 instead of 0.33, we could simply use a Young's modulus of 2.38 GPa instead of 2.5 GPa, to produce equivalent thickness estimates. It is important to highlight that the elastic properties we assume represent bulk

apparent values corresponding to the thin isotropic plate assumption, where floating ice sheets in reality are a composite sandwich material consisting of multiple ice layers of varying strength (Timco and Weeks, 2010).

290

Temperature variation over the range -20 to +2 °C would cause the speed of sound in air to vary from 318-332 m/s, resulting in ~8% variation in air-coupled flexural frequency. The effective speed of sound in air at the measurement location is also affected by wind and wind gusts may lead to variation of +/-5 m/s over timescales of minutes. However, as described in Section 4.1, we estimate the apparent velocity of the air wave for each shot, which should ensure that our air coupled flexural thickness

295   estimates are independent of changes in wind and temperature over time.

5.1 Spatial and temporal trends in ice thickness estimates

Here we give a summary of our air-coupled flexural wave ice thickness estimates for each field season and examine them in the context of borehole measurements of ice thickness and prevailing meteorological conditions, as represented by records at the nearby Sveagruva weather station (The Norwegian Meteorological institute, 2020), which was upgraded prior to the 2017

300   season to include measurement of precipitation. We assume the air-coupled flexural frequency recorded at a given geophone is related to the ice thickness at the location of the geophone, as this gave the strongest correlation with borehole thickness measurements. We also tested the assumption that the air-coupled flexural frequency represents a path averaged ice thickness between the source and receiver. However, assuming the flexural wave estimate represents the thickness at the midpoint between source and receiver gave a much poorer correlation with borehole thickness measurements.

305
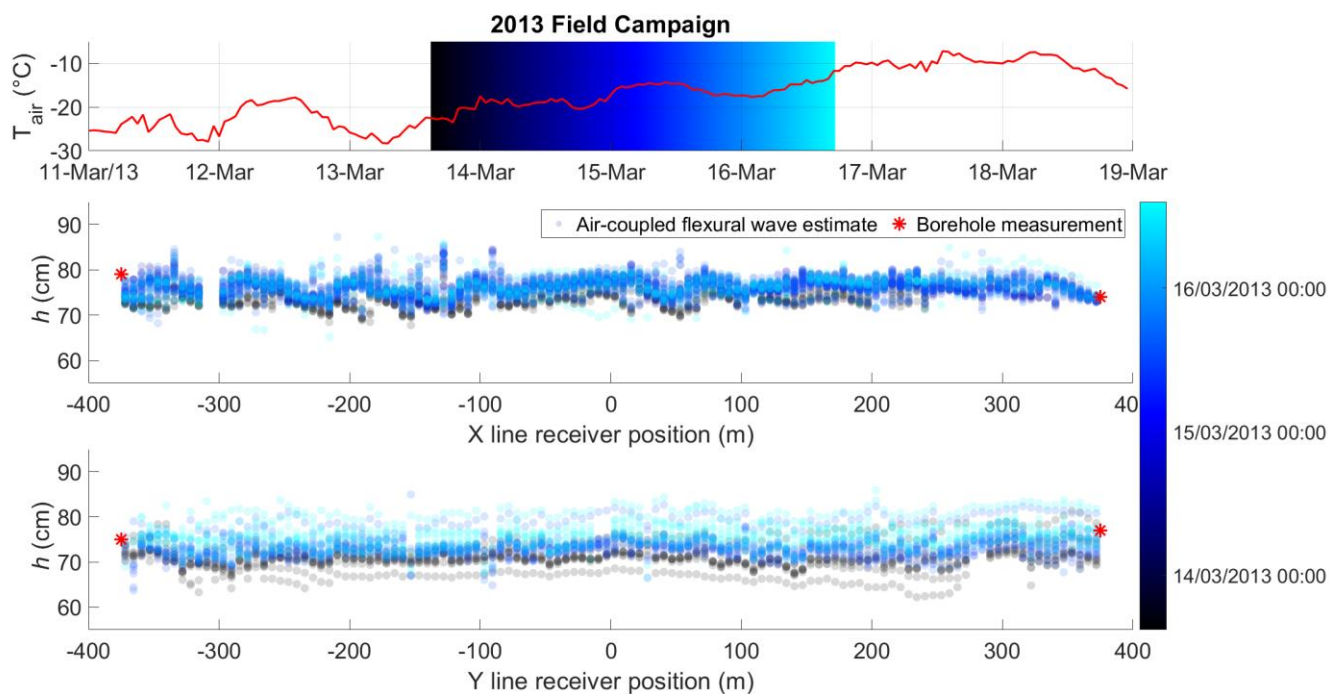
Figure 6 – 2013 field campaign air-coupled flexural wave ice thickness estimates (circles), borehole drilled thicknesses (red stars) and air temperature at nearby Sveagruva weather station (red line). The timespan of the field campaign is indicated by black-blue-cyan colour gradient. Point estimates are transparent so overlapping repeat tests are indicated by denser colours.

310

The ice thickness estimates for the 2013 field season are summarised in Figure 6 and we see good agreement between the flexural wave thickness estimates and borehole measurements. There is somewhat greater spread in the results on the Y line which is likely related to the fact that the majority of the source positions were inline with the X line and therefore oblique to the Y line (see Figure 1). The oblique geometry reduces the precision of using the linear Radon transform to estimate the

315 velocity of the air wave, which becomes smeared in the transform domain. Air temperatures remained consistently <0 °C and the thickness estimates are quite similar over the ~3 day field campaign, though there is perhaps a slight indication of ice growth with time.
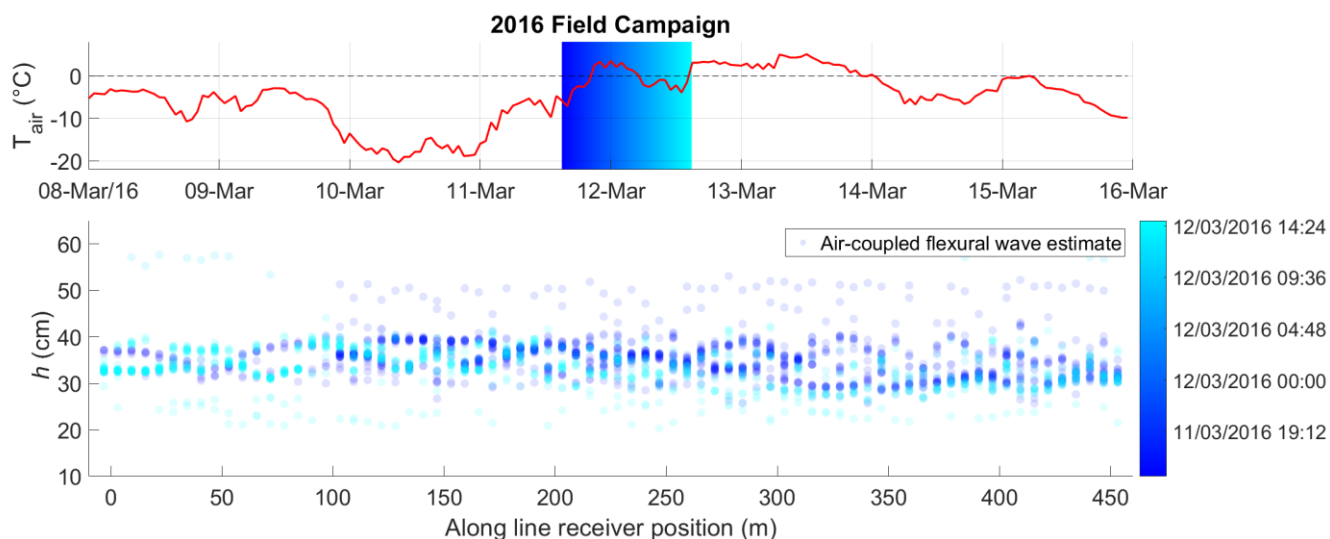
Figure 7 – 2016 field campaign air-coupled flexural wave ice thickness estimates (circles) and temperature at nearby Sveagruva weather station (red line). Timespan of field campaign is indicated by blue-cyan colour gradient. Point estimates are transparent so overlapping repeat tests are indicated by denser colours.

The results for the 2016 field season are illustrated in Figure 7. We observe some outliers in the flexural wave thickness estimates which are caused by interference of other spectral components for the extracted segment of the timeseries preceding the air-wave arrival. This interference can be due to, e.g., other wavemodes such as sub-seabed reflections, snow scooter engine noises, or instrument noise due to wind. Despite these outliers, the median thickness estimates agree well with the range of drilled thicknesses (see Table 1), although the along profile locations of the boreholes was unfortunately not recorded for this field campaign. During the field campaign, the air temperature increased to >0 °C before decreasing again. It is difficult to observe a clear trend of ice thickness variation with time, but there is perhaps some evidence for decreasing thickness, that could be due to melting during the period of >0 °C air temperature observed during the field campaign.
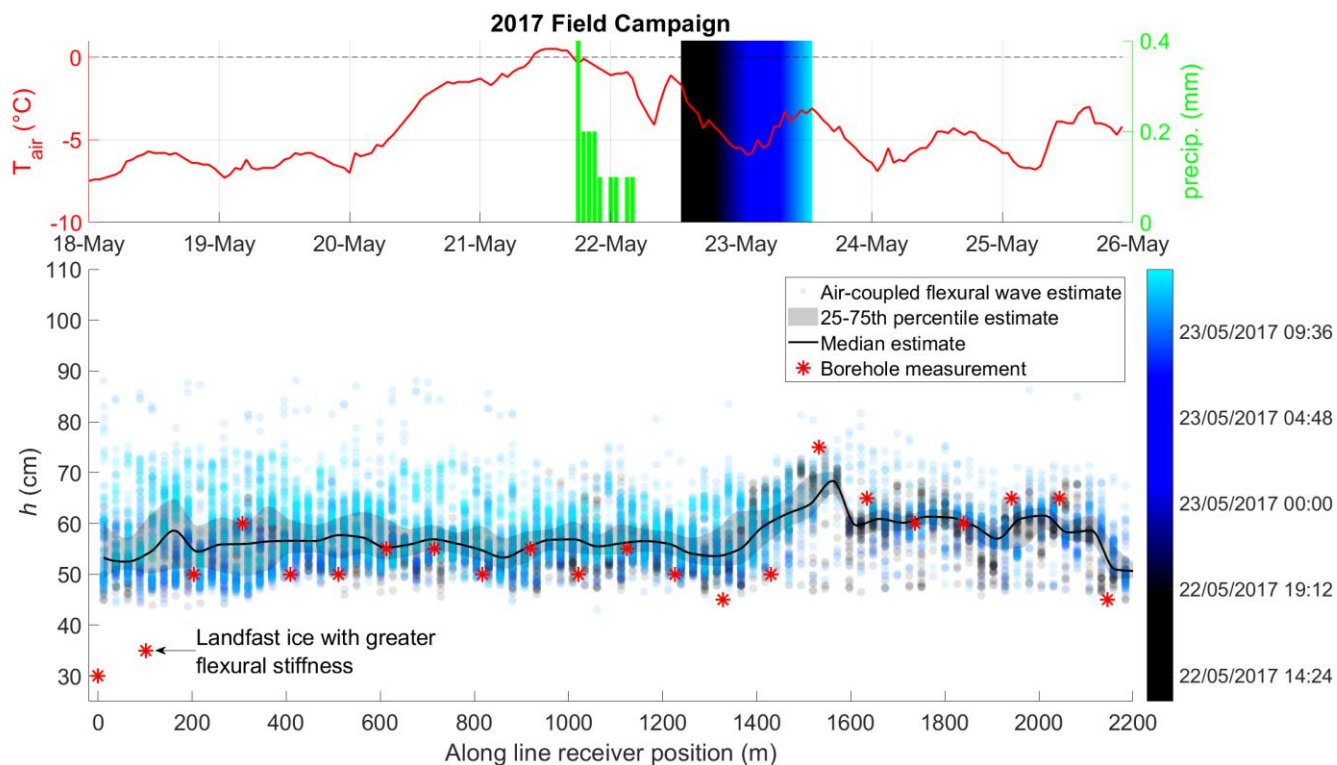
Figure 8 – 2017 field campaign (2017 L3) air-coupled flexural wave ice thickness estimates (circles), borehole drilled thicknesses (red stars), temperature (red line) and precipitation (green bars) at Sveagruva weather station. Timing is indicated by black-blue-cyan colour gradient and point estimates are transparent so overlapping repeat tests are indicated by denser colours.

335   The thickness estimates for the 2017 field season are shown in Figure 8. This field campaign was preceded by a short period of >0 °C temperatures and some precipitation, followed by a return to freezing conditions that persisted throughout the entire data collection period. We can observe that the estimated thicknesses tend to increase over the course of the field campaign, which is most evident for the shoreward portion of the line. The fact that the borehole thickness measurements, that were made while deploying the equipment prior to data recording, mostly track the lower range of ice thickness estimates gives an

340   indication that some ice growth may have occurred during the field campaign. We also observe that the estimates nearest land significantly overestimate the ice thickness relative to borehole measurements. We attribute this to the fact that the ice was landfast in the vicinity of these geophones, which gives the ice additional support and increases its flexural stiffness, making it behave as if it were thicker. Here we have chosen to use constant elastic parameters for clarity and simplicity, but the flexural ice thickness estimates could of course be improved by defining an elastic modulus that increases close to land. It is also

345   interesting to note the significant along profile variation in ice thickness recorded by the borehole measurements whose trend is also captured by the median air-coupled flexural wave thickness estimates. This is one of the main points of evidence that the frequency of air-coupled flexural waves is controlled primarily by ice thickness in the vicinity of the receiver. If we assume the air-coupled flexural waves give a thickness estimate representing the midpoint between source and receiver, we would see a flat profile with estimates ranging from ~45-75 cm with a median of ~57 cm (not included as figure) that clearly does not

350 reflect the real thickness variation recorded by the borehole measurements. By the same logic, we tested a range of assumed positions along the straight-line connecting source and receiver and found that for the spatial variation in ice thickness to be adequately represented by the air-coupled flexural wave estimates, the assumed position must be at least 98% towards the receiver.
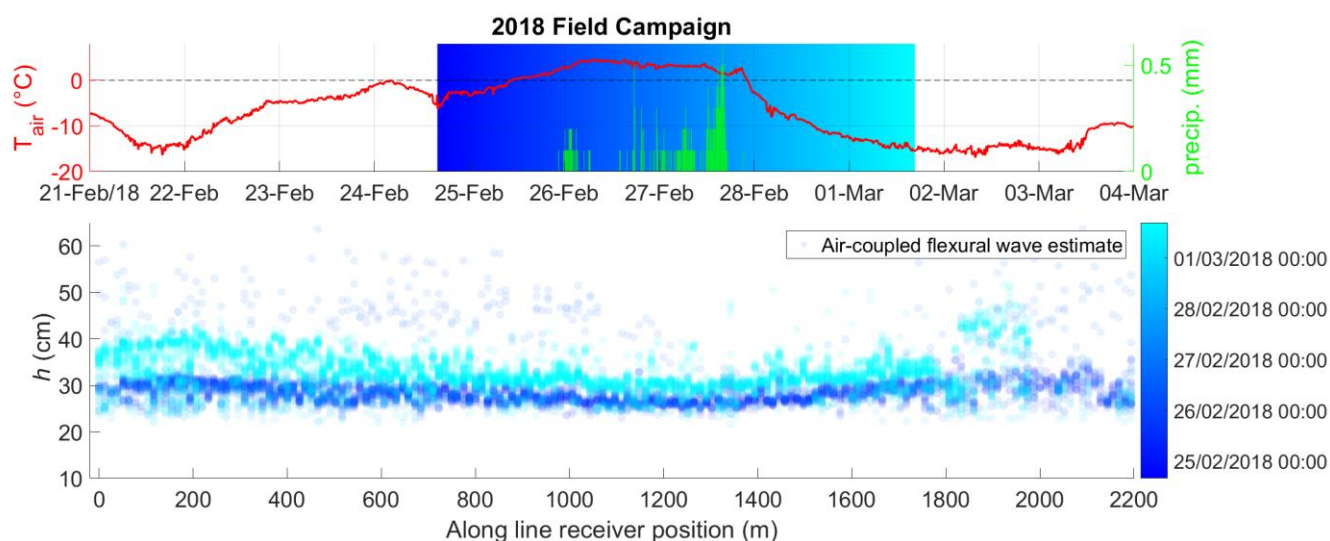
Figure 9 – 2018 field campaign air-coupled flexural wave ice thickness estimates (circles), temperature (red line) and precipitation (green bars) at Sveagruva weather station. Timing of experiments is indicated by blue-cyan colour gradient and point estimates are transparent so overlapping repeat tests are indicated by denser colours.

The air-coupled flexural wave thickness estimates for the 2018 field season are summarised in Figure 9. The thickness

360 estimates generally agree well with the range of ice thickness measured in boreholes (see Table 1), though the along profile locations of the boreholes was unfortunately not recorded for this field campaign. The most striking feature we observe for the 2018 campaign, is a clear increase in ice-thickness of up to ~10-15 cm over the course of the campaign (a period of ~4 days). This rapid increase in thickness is attributable to the weather event that occurred over 26-27th February, where >0 °C temperatures and rain led to a significant accumulation of fresh water on top of the sea ice. This event was significant enough

365 that fieldwork was not possible on the 27th February. The rapid decrease in air temperature on the 28th then promptly caused the accumulated fresh surface water to freeze, a process that occurs much more quickly than basal ice accumulation due to heat loss through the overlying ice layer, salt rejection and eventual freezing of sea water.

5.2 Solution of the full dynamical model

It is only strictly necessary to consider the solution to the dispersion relation in order to estimate ice properties from flexural

370 wave observations. However, it is also of great interest to consider the solution to the dynamical equation (Eq. (1)) in order to demonstrate that we fully understand the physics involved in the propagation of air-coupled flexural waves. To this end, we

evaluated Eq. (9) numerically using an Inverse Fast Fourier Transform (IFFT) with $N=2^{19}$ discrete points, a temporal sampling interval of $dt = 2.5 \times 10^{-4}\ s$, and a numerical attenuation/damping parameter of $\gamma = 25$. Figure 10 shows a portion of the modelled radially symmetric, expanding wavefield produced by a propagating ring delta loading that we use as an

375 approximation of the air-wave expanding outwards from a point explosive charge and pushing downwards on the ice sheet. We see that the ice sheet is deflected downwards underneath and behind the air wave, which is moving so fast that it takes some time for the ice sheet to rebound. The negative deflection decays smoothly and extends to a position around 300 m behind the load, although this is outside the figure view. Ahead of the air wave, the ice surface is elevated and we see a high, constant frequency wave-train that represents the air-coupled flexural waves. The air-coupled flexural waves decay gradually with

380 distance ahead of the load due to the inclusion of numerical damping in the model.
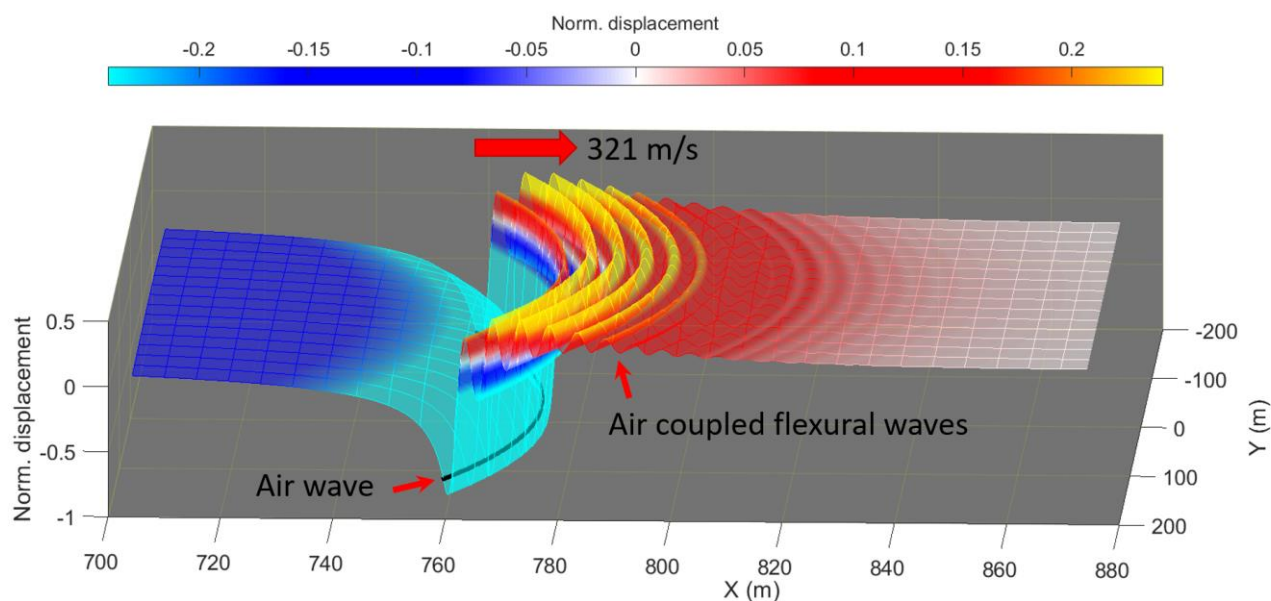
Figure 10 – Modelled normalised displacement wavefield for _h_ = 74 cm, c_{air} = 321 m/s and elastic parameters as in Table 1. The black line marks the position of the load (representing the air wave).

To compare the solutions of the full dynamical model result with field data, we calculate the velocity response of the plate at

385 a given offset by numerical time differentiation of the output from Eq. (9), and compare that directly to the recorded geophone timeseries at the same offset. We find that local velocity estimates calculated from our solutions to the dynamical model are very similar to the real waveforms recorded by geophones, as illustrated by the example in Figure 11. This increases our confidence that we understand the underlying physics that describes the excitation of air-coupled flexural waves in floating ice sheets.

390
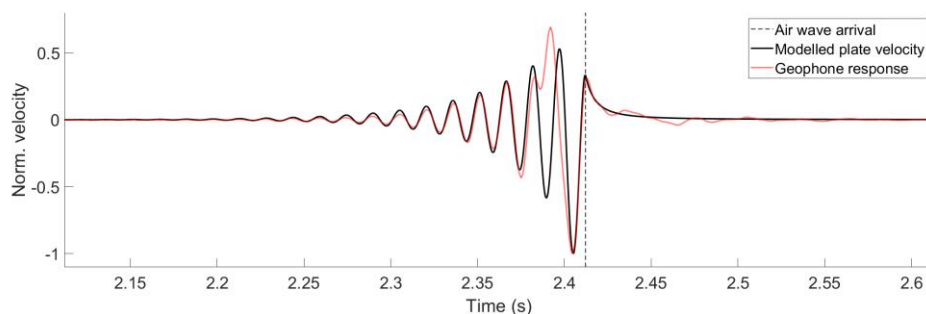
Figure 11 – Modelled normalised velocity response timeseries (black curve) at an offset of 759 m compared with the timeseries recorded by a geophone at the same offset from a point charged fired during the 2013 field season (red curve). The air wave arrival time is indicated by the dashed line.

6 Discussion

Ice flexural wave energy is commonly viewed as an undesirable class of noise that limits the ability to image sub-seabed structures at depth for seismic reflection surveys conducted on floating ice sheets (Henley, 2006; Johansen et al., 2019; Molino et al., 2008) . The high-amplitude dispersive character of the ice flexural wavefield makes it difficult to remove in reflection seismic processing so that any reflected energy arriving at the same time is masked. Inline line sources have been used in an attempt to attenuate the trailing flexural wave train (Johansen et al., 2019). However, in a classic example of the principle that one person's noise is another's signal, the ice flexural waves are very useful from the perspective of estimating the thickness and flexural stiffness of the floating ice-sheet (e.g. Timco and Weeks, 2010). An advantage of using air-coupled flexural waves in particular, is that they are readily observed for both point and inline line sources (see Figure 5). The procedure that we present in this paper is therefore applicable to a range of acquisition setups. Improved estimation of ice physical parameters may subsequently enable more efficient removal of flexural noise in reflection seismic surveys by modelling and wavefield subtraction. A direct analogue also exists for land seismic surveys where surface Rayleigh waves, commonly referred to as ground roll, couple to atmospheric compressional waves (Jardetzky and Press, 1952; Press and Ewing, 1951a).

Since we consider the air-ice-water system as fully coupled, it is possible to interpret the origin of the air-coupled flexural waves in several equivalent ways: (1) they are produced by the downward pressure of the air wave moving over the ice surface (moving loads on floating plates interpretation), (2) a plate excited by a broadband pulse propagates flexural wave energy at a range of frequencies, but sound transmission from the plate is highest at the coincidence frequency producing a resonance effect (critical/coincidence frequency interpretation), and (3) similarly, we can interpret the air-coupled flexural waves as a class of leaky Lamb waves where acoustic radiation leaks plate flexural wave energy into the air, occurring most efficiently when the phase velocity is equal to the speed of sound. The observation of air-coupled flexural waves in the absence of ice flexural waves on the far side of open water leads by Hunkins (1960) is consistent with the interpretation that, for explosive

sources on or above the ice, air coupled flexural waves are generated continuously by the downward pressure exerted by the air wave.

420 In this study, we present data acquired with linear arrays of geophones and active seismic sources that were primarily acquired to test the feasibility of seismic reflection surveying on floating sea ice. It is important to emphasize that it should also be possible to estimate and monitor ice properties with much simpler equipment. Indeed, from our results we would expect that a simple microphone, sensitive in the relevant frequency range and located in the vicinity of the desired measurement, either above the ice-sheet or along the shoreline would be sufficient. The microphone response in air could be modelled by adapting
425 the present model to include the acoustic emission from the plate based on plate transmission loss theory (Long, 2014), though the air coupled flexural frequency will remain unchanged. The potential to monitor ice thickness using a microphone positioned on land would be a great benefit from the perspective of continuous environmental monitoring, particularly early in the freezing season when the ice is too thin to be safely traversed.

430 Our results indicate that air-coupled flexural waves can be used to resolve spatial and temporal ice thickness variation. Some degree of scatter is observed in our thickness estimates, but the median of repeated measurements appears to give a reliable estimation. A small percentage of outliers are present in the thickness estimates, that we attribute to spectral contamination caused by the simultaneous arrival of other wave modes with the air-coupled flexural waves. Such interference was minimised by discarding the nearest offsets where high-velocity sub-seabed reflections arrive at the same time as the air wave (see Figure
435 5). However, other noise sources, such as snow scooter traffic, are difficult to avoid in real-world data. In the rare cases that traffic noise is recorded at the same instant as the air-coupled flexural waves, the resulting spectral interference can prevent accurate estimation of the air-coupled flexural frequency. It is also important to highlight that the air-coupled flexural frequency is affected by the elastic properties of the ice, it's flexural rigidity, not just it's thickness. By assuming a constant set of elastic parameters our thickness estimates may be considered "effective thicknesses" corresponding to the assumed
440 elastic parameters and subject to the thin isotropic plate assumption. However, we also expect that the "effective thickness" for assumed elastic properties is still highly relevant when assessing the load bearing capacity of floating ice, even if it were to deviate from the true thickness.

In the present study, the receiver array is utilized to measure the apparent sound velocity in air across the array. The sound
445 velocities we estimated were generally consistent with the expected sound speeds based on air temperature measured at the nearby Sveagruva weather station. However, the apparent sound velocity is also affected by horizontal wind velocity (e.g. Franke and Swenson Jr, 1989), which likely explains why the array estimates can vary by ~3 m/s over timescales of a few minutes. For the case of a simpler recording system, such as a single microphone, it may still be possible to adequately constrain the sound velocity using measurements of temperature, wind speed and direction.

450

While detonating cord seismic sources were used for the experiments presented in this study, other impulsive sources acting on a floating ice-sheet also have the potential to excite air-coupled flexural waves. For example, crack propagation in a plate produces a sudden energy release that is capable of exciting propagating elastic waves in the plate and acoustic pressure waves in air. This phenomenon has been studied from the structural non-destructive testing perspective, e.g., by Haider and Giurgiutiu

455 (2018) who model the acoustic emission of axis symmetric circular crested Lamb waves excited by crack propagation in a steel plate. Ice quakes produced by the sudden cracking of floating ice are a well-known phenomenon (Kavanaugh et al., 2019; Olinger et al., 2019; Ruzhich et al., 2009) and are typically related to the build-up of stress by thermal, tidal and wind forces. The excitation of air-coupled flexural waves by cracks in floating ice sheets is also familiar to ice skaters traversing frozen rivers and lakes, whose body weight is enough to flex the ice and cause cracks to form when it is very thin (e.g. Rankin, 2018).

460 The excitation of air-coupled flexural waves by natural crack formation/propagation in floating ice sheets raises the possibility of passive monitoring of ice thickness and rigidity.

To highlight that the otherworldly sounds familiar to ice skaters are air-coupled flexural waves, simply shifted to higher frequencies because of the thinner, stiffer fresh-water ice, we examined the spectrogram of the audio track from the National

465 Geographic short film "How Skating on Thin Ice Creates Laser-Like Sounds" (Rankin, 2018). The frequency of the sounds varies within the 700-800 Hz, lying around 725 Hz for the example shown in Figure 12. Using Eq. 15 we calculate that the ice was ~4.3 cm thick, assuming Young's modulus of 8.5 GPa, Poisson's ratio of 0.33, water density of 1000 kg/m^3, ice density of 917 kg/m^3, water depth of at least 0.3 m and sound speed of 329 m/s corresponding to air temperature of -3.9 °C. This is in line with the measured ice thickness presented in the film and illustrates the potential to use air-coupled flexural waves recorded

470 by a simple microphone to estimate ice properties.
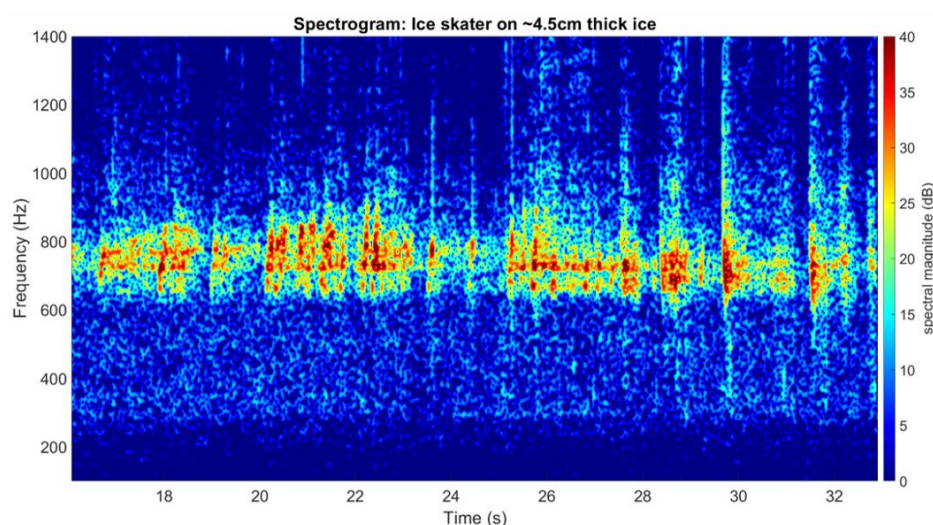
Figure 12 – Spectrogram of audio track from a segment of the National Geographic short film "How Skating on Thin Ice Creates Laser-Like Sounds" (Rankin, 2018).

475 The air-coupled flexural wave phenomenon in floating ice is one example of the more general concept of moving loads on floating plates. We emphasize the theoretical similarity between this study and the larger field of study around moving vehicles on floating plates. There is also significant overlap with the fields of structural acoustics and non-destructive testing, where an analogous phenomenon is described by the concept of coincidence frequency. These concepts can be generalised even further to the field of pulse propagation in coupled systems, recalling for example the air-sea waves produced by the eruption of

480 Krakatoa that was discussed in the introduction.

7 Conclusion

Air-coupled flexural waves are a robust feature of floating ice-sheets excited by impulsive sources over a large range of thicknesses. The physics of these waves can be understood from a theoretical perspective that has largely developed through the study of moving vehicles on floating plates. The dynamical model that we favour is straightforward to understand in terms

of linear filter theory, and we derived a closed-form solution of the dispersion relation that relates ice thickness directly to the air-coupled flexural wave frequency and air-wave velocity. We tested the proposed closed-form ice thickness estimator extensively on field data from four field seasons, and found a remarkably good agreement with in-situ borehole measurements. The phenomenon of air-coupled flexural waves is relatively familiar to the wild ice-skating community, where thin ice produces air-coupled flexural waves that are readily audible (and fascinatingly otherworldly). Here we build on the pioneering efforts of Press and Ewing (1951b), developing a more accessible theory supported by modern numerical and Fourier transform methods, to show that the same phenomenon also occurs for much thicker sea-ice, simply shifted to a lower frequency regime. We have mainly presented data that was acquired for the primary purpose of reflection seismic profiling, but a key benefit of air-coupled flexural waves is that they should also be recordable with very simple equipment, such as a microphone located in the vicinity of where a thickness measurement is desired, either above the ice-sheet or along the shoreline. Cracks in the ice, either produced artificially by, e.g., ice skates on thin ice, or naturally occurring, represent possible alternative impulsive sources capable of exciting air-coupled flexural waves.

8 Code and data availability

Data and code used to produce this research can be shared upon request to the authors.

9 Author contributions

Development of theory and associated modelling was carried out by RR and AH. The field campaigns were administered and led by TAJ and BOR. Initial data preparation was conducted by BOR, while the air-coupled flexural wave data processing methodology was developed and implemented by RR. RR was responsible for analysing and visualising the data and writing the manuscript with contributions from all authors

10 Competing interests

The authors declare that they have no conflict of interest.

11 Financial support

This research has been supported by the University of Tromsø – The Arctic University of Norway, ARCEx partners and the Research Council of Norway (grant no. 228107). The publication charges for this article have been funded by a grant from the publication fund of UiT The Arctic University of Norway.

12 References

Bhattacharya, M., Guy, R., and Crocker, M.: Coincidence effect with sound waves in a finite plate, Journal of sound and vibration, 18, 157-169, 1971.

DiMarco, R., Dugan, J., Martin, W., and Tucker III, W.: Sea ice flexural rigidity: a comparison of methods, Cold regions science and technology, 21, 247-255, 1993.

Dinvay, E., Kalisch, H., and Părău, E.: Fully dispersive models for moving loads on ice sheets, J Fluid Mech, 876, 122-149, 2019.

Ewing, M. and Crary, A.: Propagation of elastic waves in ice. Part II, Physics, 5, 181-184, 1934.

Ewing, M. and Press, F.: Tide-gage disturbances from the great eruption of Krakatoa, Eos, Transactions American Geophysical Union, 36, 53-60, 1955.

Franke, S. J. and Swenson Jr, G.: A brief tutorial on the fast field program (FFP) as applied to sound propagation in the air, Applied Acoustics, 27, 203-215, 1989.

Garrett, C.: A theory of the Krakatoa tide gauge disturbances, Tellus, 22, 43-52, 1970.

Greenhill, A.: Wave motion in hydrodynamics, American Journal of Mathematics, 1886. 62-96, 1886.

Greenhill, G.: I. Skating on thin ice, The London, Edinburgh, and Dublin Philosophical Magazine and Journal of Science, 31, 1-22, 1916.

Griffin, J.: The Magic (and Math) of Skating on Thin Ice without Falling In. Scientific American, 2018.

Haider, M. F. and Giurgiutiu, V.: Analysis of axis symmetric circular crested elastic wave generated during crack propagation in a plate: A Helmholtz potential technique, International Journal of Solids and Structures, 134, 130-150, 2018.

Harkrider, D. and Press, F.: The Krakatoa Air—Sea Waves: An Example of Pulse Propagation in Coupled Systems, Geophysical Journal International, 13, 149-159, 1967.

Haskell, N. A.: A note on air-coupled surface waves, Bulletin of the Seismological Society of America, 41, 295-300, 1951.

Henley, D. C.: Attenuating the ice flexural wave on arctic seismic data. In: SEG Technical Program Expanded Abstracts 2006, 2006.

Hinchey, M. and Colbourne, B.: Research on low and high speed hovercraft icebreaking, Canadian Journal of Civil Engineering, 22, 32-42, 1995.

Hunkins, K.: Seismic studies of sea ice, Journal of Geophysical Research, 65, 3459-3472, 1960.

Jardetzky, W. S. and Press, F.: Rayleigh-wave coupling to atmospheric compression waves, Bulletin of the Seismological Society of America, 42, 135-144, 1952.

Johansen, T. A., Ruud, B. O., Tømmerbakke, R., and Jensen, K.: Seismic on floating ice: data acquisition versus flexural wave noise, Geophysical Prospecting, 67, 532-549, 2019.

Kashiwagi, M.: Transient responses of a VLFS during landing and take-off of an airplane, Journal of marine science and technology, 9, 14-23, 2004.

Kavanaugh, J., Schultz, R., Andriashek, L. D., van der Baan, M., Ghofrani, H., Atkinson, G., and Utting, D. J.: A New Year's Day icebreaker: icequakes on lakes in Alberta, Canada, Canadian Journal of Earth Sciences, 56, 183-200, 2019.

Kozin, V., Zemlyak, V., and Rogozhnikova, E.: Increasing the efficiency of the resonance method for breaking an ice cover with simultaneous movement of two air cushion vehicles, Journal of Applied Mechanics and Technical Physics, 58, 349-353, 2017.

Kozin, V. M. and Pogorelova, A. V.: Submarine moving close to the ice-surface conditions, 2008.

Long, M.: Sound Transmission Loss. In: Architectural acoustics, Elsevier, 2014.

Matiushina, A. A., Pogorelova, A. V., and Kozin, V. M.: Effect of impact load on the ice cover during the landing of an airplane, International Journal of Offshore and Polar Engineering, 26, 6-12, 2016.

Miles, J. and Sneyd, A. D.: The response of a floating ice sheet to an accelerating line load, J Fluid Mech, 497, 435-439, 2003.

Molino, G. D., Rovetta, D., Mazzucchelli, P., Sandroni, S., Rizzo, F., and Andreoletti, C.: Seismic exploration on ice: the flexural wave noise challenge. In: SEG Technical Program Expanded Abstracts 2008, Society of Exploration Geophysicists, 2008.

Nickalls, R. W.: A new approach to solving the cubic: Cardan's solution revealed, The Mathematical Gazette, 77, 354-359, 1993.

Nugroho, W. S., Wang, K., Hosking, R., and Milinazzo, F.: Time-dependent response of a floating flexible plate to an impulsively started steadily moving load, J Fluid Mech, 381, 337-355, 1999.

Olinger, S., Lipovsky, B., Wiens, D., Aster, R., Bromirski, P., Chen, Z., Gerstoft, P., Nyblade, A. A., and Stephen, R.: Tidal and thermal stresses drive seismicity along a major Ross Ice Shelf rift, Geophysical Research Letters, 46, 6644-6652, 2019.

Press, F., Crary, A., Oliver, J., and Katz, S.: Air-coupled flexural waves in floating ice, Eos, Transactions American Geophysical Union, 32, 166-172, 1951.

Press, F. and Ewing, M.: Ground roll coupling to atmospheric compressional waves, Geophysics, 16, 416-430, 1951a.

Press, F. and Ewing, M.: Theory of air-coupled flexural waves, Journal of Applied Physics, 22, 892-899, 1951b.

Press, F. and Oliver, J.: Model study of air-coupled surface waves, The Journal of the Acoustical Society of America, 27, 43-46, 1955.

Rankin, A.: How Skating on Thin Ice Creates Laser-Like Sounds. In: National Geographic, National Geographic, 2018.

Renji, K., Nair, P., and Narayanan, S.: Critical and coincidence frequencies of flat panels, Journal of sound and vibration, 205, 19-32, 1997.

Ruzhich, V., Psakhie, S. G., Chernykh, E., Bornyakov, S., and Granin, N.: Deformation and seismic effects in the ice cover of Lake Baikal, Russian Geology and Geophysics, 50, 214-221, 2009.

Schulkes, R. M. S. M. and Sneyd, A. D.: Time-dependent response of floating ice to a steadily moving load, J Fluid Mech, 186, 25-46, 1988.

Squire, V., Hosking, R. J., Kerr, A. D., and Langhorne, P.: Moving Loads on Ice Plates, Springer Science & Business Media, 1996.

Takizawa, T.: Response of a floating sea ice sheet to a steadily moving load, Journal of Geophysical Research: Oceans, 93, 5100-5112, 1988.

The Norwegian Meteorological institute: Norsk Klimaservicesenter - Observations and weather statistics. 2020.

570 Thomson, D. J.: Spectrum estimation and harmonic analysis, Proceedings of the IEEE, 70, 1055-1096, 1982.

Timco, G. W. and Weeks, W. F.: A review of the engineering properties of sea ice, Cold Regions Science and Technology, 60, 107-129, 2010.

Van der Sanden, J. and Short, N.: Radar satellites measure ice cover displacements induced by moving vehicles, Cold Regions Science and Technology, 133, 56-62, 2017.

575 Wang, K., Hosking, R., and Milinazzo, F.: Time-dependent response of a floating viscoelastic plate to an impulsively started moving load, J Fluid Mech, 521, 295, 2004.

Wilson, J. T.: Coupling between moving loads and flexural waves in floating ice sheets, U.S. Army Snow, Ice, and Permafrost Research Establishment. SIPRE technical report no. 34., 1955.

Yang, T. C. and Yates, T. W.: Flexural waves in a floating ice sheet: Modeling and comparison with data, The Journal of the Acoustical 580 Society of America, 97, 971-977, 1995.

Yeung, R. and Kim, J.: Effects of a Translating Load on a Floating Plate—Structural Drag and Plate Deformation, Journal of fluids and structures, 14, 993-1011, 2000.

Yilmaz, Ö.: Seismic data analysis: Processing, inversion, and interpretation of seismic data, Society of exploration geophysicists, 2001.

Zhu, J.: Non-contact NDT of concrete structures using air coupled sensors, Newmark Structural Engineering Laboratory. University of 585 Illinois at Urbana. Report No. NSEL-010, 2008.